Journal of Energy Storage 86 (2024) 111289

Contents lists available at ScienceDirect

Journal of Energy Storage

journal homepage: www.elsevier.com/locate/est

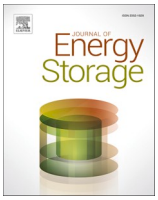

Research papers

An experimental investigation of liquid immersion cooling of a four cell lithium-ion battery module

N.P. Williams *, D. Trimble, S.M. O'Shaughnessy

Department of Mechanical, Manufacturing, and Biomedical Engineering, Trinity College, University of Dublin, Ireland

ARTICLE INFO

Keywords:
Immersion cooling
Electric vehicles
Fast charging
Dielectric liquid
Battery thermal management
Two-phase cooling

ABSTRACT

The thermal management of a lithium-ion battery module subjected to direct contact liquid immersion cooling conditions is experimentally investigated in this study. Four 2.5 Ah 26650 $LiFePO_4$ cylindrical cells in a square arrangement and connected electrically in parallel are completely immersed in the dielectric fluid Novec 7000. The thermal and electrical behaviour of the module is assessed at charging and discharging rates of 1C to 4C. Experiments are conducted with initially ambient temperature liquid, resulting in single phase natural convection cooling, as well as preheated liquid temperatures of 33 °C ± 0.5 °C to study the influence of the phase change process under pool boiling conditions. Superior performance is observed when two-phase immersion cooling conditions are established for discharge rates of 2C and above, limiting the average cell temperature rise to 1.9 °C at the end of 4C discharge, corresponding to a maximum temperature of 34.7 °C. For the most onerous charging rate of 4C, considered fast charging, this maximum temperature rise is limited to 1.3 °C, corresponding to a maximum temperature of 35 °C. Vigorous boiling is observed from the cells' electrodes, leading to more effective heat transfer from the locations of high heat flux. Excellent module thermal homogeneity is exhibited, maintaining a maximum temperature difference of 1.2 °C for all cases investigated. The axial temperature gradients of the module's individual cells are also greatly reduced under two-phase conditions. The influence of cell spacing within the module is also investigated for inter-cell spacings of 0.25*D* and 1*D*, where *D* is the cell diameter. Marginally improved heat transfer performance is observed for the more closely spaced cell arrangements, reducing the maximum cell temperatures and thermal inhomogeneity within the module.

1. Introduction

A wider adoption of electric vehicles (EV) has been targeted by many organisations and governments to meet various emission and climate-related goals. It is long established that the lithium-ion cells of production level EV operate optimally within a narrow temperature range between 25 °C and 40 °C [1]. Further requirements to maintain temperature differences within individual cells below 2 °C [2] and between cells within a module to less than 5 °C [1] pose significant challenges to current battery thermal management systems (BTMS). Failure to meet these temperature criteria can result in poor battery pack performance including reduced capacity [3] and lifespan, coupled with safety concerns such as thermal runaway.

The heat generated by lithium-ion cells is dependent on numerous factors including their electrochemistry, capacity, charge/discharge rate, geometry, state of charge (SOC), and environmental conditions. The thermal management challenge is likely to become increasingly difficult as future battery technologies are predicted to result in smaller, lighter, more energy dense cells [4] and battery packs of increased power density. These thermal limits are antagonistic to consumer demand for faster pack charging to bring 'refuelling' times in line with those of internal combustion engine (ICE) vehicles. Greater heat generation rates within the battery pack are associated with fast charging, in which cells are charged to 80 % of their final capacity within 15 minutes [5], placing further demand on any BTMS.

Previous and current BTMS approaches employed in production EV have included passive [6] and forced air cooling [7], as well as indirect contact liquid cooling utilising heat spreading devices such as cold plates containing minichannels [8] or microchannels [9]. Despite attempts to improve its performance, air cooling is proven to be unsuitable for maintaining the required thermal limits at high discharge rates or unfavourable ambient conditions [10]. Furthermore, the thermal contact resistances associated with the heat spreading devices of indirect contact liquid cooling are detrimental to heat transfer, which would only be further exacerbated at elevated charging/discharging rates. Several

* Corresponding author.
E-mail address: nwilliam@tcd.ie (N.P. Williams).

https://doi.org/10.1016/j.est.2024.111289
Received 22 November 2023; Received in revised form 20 January 2024; Accepted 10 March 2024
Available online 23 March 2024
2352-152X/© 2024 The Authors. Published by Elsevier Ltd. This is an open access article under the CC BY license (http://creativecommons.org/licenses/by/4.0/).

Nomenclature

C	Cell C-rate, $1/h$
C_{cell}	Cell capacity, Ah
D	Diameter, m
$\frac{dU}{dT}$	Entropic heat coefficient, V/K
I	Current, A
δT	Temperature difference, $^{\circ}C$ *or* K
ΔT	Temperature rise, $^{\circ}C$ *or* K
t	Time, s
V	Voltage, V

Subscript

avg	Average
cell	Cell
i, j	Cell number
max	Maximum
min	Minimum
module	Module
0	Initial

Greek symbol

η	Overpotential, V

Acronyms

BTMS	Battery thermal management systems
CC	Constant current
CV	Constant voltage
DAQ	Data acquisition module
DOD	Depth of discharge
EV	Electric vehicles
HFE	Hydrofluoroether
HFO	Hydrofluoroolefin
ICE	Internal combustion engine
LFP	Lithium iron phosphate
NCA	Lithium nickel cobalt aluminium oxide
OCV	Open circuit voltage, V
PCM	Phase change material
SEI	Solid electrolyte interphase
SOC	State of charge

alternate BTMS have been proposed in literature, including phase change materials (PCM) [11] and heat pipes [12]. However, poor performance has been observed with these methods, such as operating temperature requirements above the 40 °C limit and module temperature differences far in excess of 5 °C.

To facilitate greater heat transfer rates under more onerous operating conditions, direct contact liquid immersion cooling is receiving increased attention in both academic literature and industry. In this BTMS, cells are immersed in an electrically non-conductive dielectric fluid. This method can result in improved spatial and temporal temperature uniformity and offer increased safety in thermal runaway events.

A number of studies have investigated the use of high viscosity dielectric fluids for direct contact battery thermal management under both natural and forced convection single phase conditions, including mineral oils, ester oils and those traditionally used in transformers. While the maximum temperatures of individual prismatic [13] and cylindrical cells [14] were maintained below 40 °C for discharge rates of up to 3C (where C is the ratio of operating current to rated cell capacity), poor thermal homogeneity was observed for cylindrical cell module arrangements with small inter-cell spacings ($\leq$ 2 mm), far exceeding the 5 °C acceptable limit [15]. Increased cell spacings and flow rates in excess of 0.4 L/min [16] maintained desirable thermal homogeneity within cylindrical cell modules, while similar flow rates were required by Wang et al. [17] to prevent the maximum temperature within a prismatic pouch cell module from exceeding 40 °C. For a module consisting of 14 prismatic pouch cells which combined forced convection air cooling at the tabs and immersion of the cells' bodies as proposed by Patil et al. [18], flow rates greater than 3 L/min and inlet air velocities of 5 m/s were necessary to maintain thermal uniformity. These increased flow rates to limit thermal inhomogeneity are coupled with greater pressure drops due to the fluids' highly viscous nature. A drop contact cooling method was proposed by Zha et al. [19] in which a transformer oil was introduced at flow rates of up to 20 mL/min above the centre of 3.4 Ah 18650 lithium nickel cobalt aluminium oxide (NCA) cells arranged in a 21 cell module. Greater thermal performance was observed in comparison to fully immersed forced convection single phase conditions, maintaining a maximum cell temperature of 37.23 °C for a 2C discharge rate. A maximum temperature difference across the module of 1.1 °C was observed experimentally at a discharge rate of 1C. However, a difference of approximately 1.9 °C across the individual cells was determined from numerical simulations, approaching the limit for degradation minimisation.

The use of dielectric fluids with lower viscosities such as the hydrofluoroethers (HFE) Novec 7200 [20,21] and Novec 7500 [22] can improve the thermal homogeneity within module arrangements as heat transfer is increased due to heightened mixing of the fluid, particularly under single phase natural convection conditions. The cells' thermal limits have been maintained for a small cylindrical cell module immersed in Novec 7200 at cycling rates of up to 3C under natural convection conditions by Liu et al. [20], as well as a module of 25 cells cycled at the low rate of 1.33C for over 1000 cycles by Koster et al. [21] when characterising cell degradation under forced convection single phase conditions in the same fluid. The desired thermal homogeneity was also maintained by Solai et al. [23] for the immersion of eight cylindrical cells in the dielectric fluid CFX70 at the onerous cycling rate of 10C, albeit for extremely short cycle durations of 10 s. To improve heat transfer to the surrounding Novec 7500 fluid, a hybrid BTMS was proposed by Choi et al. [22] for a prismatic pouch cell module in which the spacing between each cell contained graphite fins. Slightly improved thermal performance was observed for this hybrid BTMS in comparison to a fluid-only arrangement, though the thermal homogeneity remained close to allowable limits. A flow rate of approximately 1.9 L/min was required for the hybrid system, resulting in a lower pressure drop across the module against the fluid-only arrangement. However, for larger modules of cylindrical cells at discharge rates $\geq$ 2C, flow rates $\leq$ 1 L/min were found to be insufficient to successfully manage the cells' temperature which exceeded 60 °C at the end of 4C discharge, accompanied by a temperature difference of 16.8 °C across the module for immersion in the fluid E5-TM410 [24].

To further improve the performance of direct contact liquid immersion cooling, the use of dielectric fluids with phase change temperatures within the desirable operating limits has received increasing attention due to the high rates of heat transfer and thermal homogenisation offered by the latent heat of phase change.

Studies have predominantly examined the performance of single cells under static immersion conditions in the dielectric fluid Novec 7000, which has a saturation temperature of 34 °C. For discharge rates of up to 3C [25] and pulse charge-discharge cycling at 5C [26], the temperature rise of single cells was reduced significantly in comparison to natural convection conditions, with vapour bubble nucleation during phase change concentrated at the cells' electrodes. Similar performance was observed by Li et al. [27] at a maximum discharge rate of 7C for cell immersion in the hydrofluoroolefin (HFO) SF33, which has similar

thermophysical properties to Novec 7000. Module arrangements of cylindrical cells at 3C discharge [28] and low capacity prismatic pouch cells at the extreme discharge rates of 10C and 20C [29] have also been investigated for immersion in Novec 7000, with temperature differences of less than 1 °C observed across these modules.

This thermal management method has also been subjected to fast charging conditions by Li et al. [30] investigating the performance of cylindrical cells of varying geometry and electrochemistry when immersed in SF33, with the maximum temperature rise limited to 3.4 °C during 3C charging. The authors later immersed a module of 21 cylindrical cells in the dielectric fluid SF49 [31], with the temperature rise and module inhomogeneity limited to 4.8 °C and 1 °C respectively during more onerous 4C charging. The current authors' previous study on two-phase immersion cooling of single cylindrical cells in Novec 7000 restricted their temperature rise under onerous 10C discharge and 4C charge conditions to 3.6 °C and 1 °C respectively [32]. The effect of cylindrical cell to cell spacing within a module was investigated numerically by Al-Zareer et al. in their work on a hybrid electric vehicle (HEV) system featuring two-phase immersion cooling with propane [33] as the working fluid. However, the dynamics of the phase change process were not modelled, with empirical correlations applied to replicate the increased heat transfer rates of the boiling process.

The application of flow boiling to battery thermal management has also been investigated by Wang and Wu [34] for a large module arrangement consisting of 60 cylindrical cells immersed in Novec 7000, with low vapour fractions at the module's outlet required to reduce the maximum cell temperature and improve thermal homogenisation. The authors later examined cell performance when ethanol was added to the low boiling point refrigerant R1233zd(E) to improve its thermal properties [35]. Boiling from the cells' walls was observed to depart from the nucleate regime for refrigerant volume fractions in excess of approximately 0.8, increasing the vapour volume fraction at the outlet and subsequently the temperature difference across the module.

Despite the promising performance of this method of battery thermal management, the majority of two-phase immersion cooling studies have been performed experimentally for a single cell solely charging or discharging at high rates, with limited work on module arrangements which investigate the thermal homogeneity purportedly offered by this proposed BTMS. Furthermore, in a number of these studies an open immersion vessel is used to maintain saturation conditions, with no method of vapour condensation. This is unrealistic of real battery module applications, with the liquid level varying throughout the charging and/or discharging process. In certain cases, in which the module is a sealed system, the absence of a condensation or cooling mechanism leads to a pressure increase and subsequently varying saturation conditions.

1.1. Research aim and objectives

This study aims to experimentally determine the effectiveness of liquid immersion cooling for battery thermal management by investigating the electrical and thermal performance of a battery module consisting of four lithium iron phosphate (LFP or $LiFePO_4$) cylindrical cells. The thermal homogeneity and maximum cell temperature of the module is compared under single phase natural convection and two-phase immersion conditions for both charging and discharging rates of up to 4C, placing the cells under onerous operating conditions. The effect of cell spacing on performance, thermal uniformity in particular, is examined, which to the authors' knowledge has not been previously studied experimentally for cylindrical cells. These findings can inform future designs of two-phase immersion cooling systems.

2. Experimental method

2.1. Test chamber

The experimental set-up consists of a central test chamber and auxiliary flow loop, as illustrated in Fig. 1. The lithium-ion cell module is housed in a 316L stainless steel chamber of 0.1 m × 0.1 m × 0.2 m internal dimensions, as illustrated in Fig. 2, assembled with Viton (FKM) rubber seals which were found to have good material compatibility with the working fluid. While Viton is slightly fluorinated, no reaction has been detected with the working fluid. However, the time period over which a reaction between the two materials takes place may be such that it has yet to be detected. Power and sensor connections pass through cable glands containing compatible seals to minimise liquid loss from the chamber and are wrapped in a suitable heat shrink material to further prevent contamination of the working fluid. The chamber is also insulated to minimise heat loss. The experimental set-up is discussed in greater detail in the authors' previous work on single cell immersion cooling [32].

The module consists of four 2.5 Ah LithiumWerks ANR26650M1B 26650 $LiFePO_4$ cylindrical cells connected electrically in a 1 in series, 4 in parallel (1s, 4p) configuration via copper busbars. The module's nominal capacity is therefore 10 Ah, such that a C rate of 1C refers to a charge/discharge current of 10 A. Power connections to the busbars are made through 6 mm^2 tri-rated cable. The module's cells, each of diameter D, are arranged in a square array, with equally spaced horizontal and vertical cell wall-to-wall distances. In this study, spacing distances of 0.25D and 1D are investigated, as presented in Fig. 3. The orientation of the module is such that the cells' positive electrodes are closest to the surface of the liquid pool. Additional cell details are available in Table 1.

The module is completely immersed in approximately 0.81 L of the dielectric fluid Novec 7000 which has a saturation temperature of 34 °C, within the operating temperature range for lithium-ion cells. The fluid is degassed under ambient temperature and pressure conditions by circulation through a membrane contactor via a canned pump, with the vacuum applied across the membrane removing the dissolved air. The degassing loop, as well as a schematic of the complete experimental set-up, is presented in Fig. 4. Further details on the working fluid are outlined in Table 2. Due to their high electrochemical efficiency, lithium-ion cells produce relatively low heat generation rates. Combined with the low specific heat capacity and thermal conductivity of the coolant fluid, two polyimide film auxiliary heaters (Omega KHLVA-104/10-P) are required for fluid preheating to 33 °C ± 0.5 °C to study the module's response during two-phase flow and heat transfer conditions. The temperature of all cells and bulk fluid is monitored throughout the preheating process, with the heating power adjusted until the required preheating temperature is reached. Upon a steady state being established during which the temperature fluctuations stabilise, charging and discharging under preheated conditions commences.

For all tests, an 8 mm outer diameter copper coil supplied with water at 15 °C ± 0.1 °C and a flow rate of 3.7 L/min ± 0.1 L/min by a Thermo Scientific Accel LC 500 recirculating chiller condenses vapour produced during the phase change process. The typical fluctuation of the cooling water temperature is less than 0.1 °C, which is the precision of the recirculating chiller. An Omega PXM319 pressure transducer monitors the saturation conditions. The module's voltage and system pressure are recorded by a National Instruments (NI) 9219 data acquisition module (DAQ).

Five T-type exposed junction thermocouples are spaced 11 mm apart along each cell's primary axis, affixed using OMEGABOND 101 high conductivity thermal adhesive. The cell surface averaged temperature $T_{i,avg}$, where i is the cell number, is determined from the average of their instantaneous measurements. The liquid pool and vapour temperatures are monitored by 1.5 mm diameter T-type stainless steel thermocouple probes. All temperature measurements are recorded using NI 9213 and

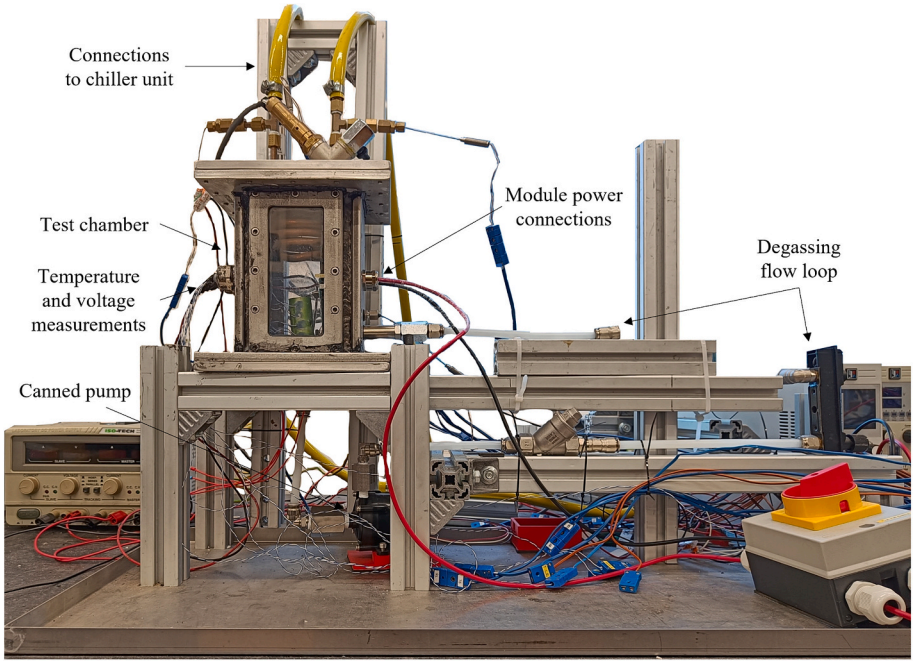

Fig. 1. Experimental set-up, including test chamber and degassing flow loop.

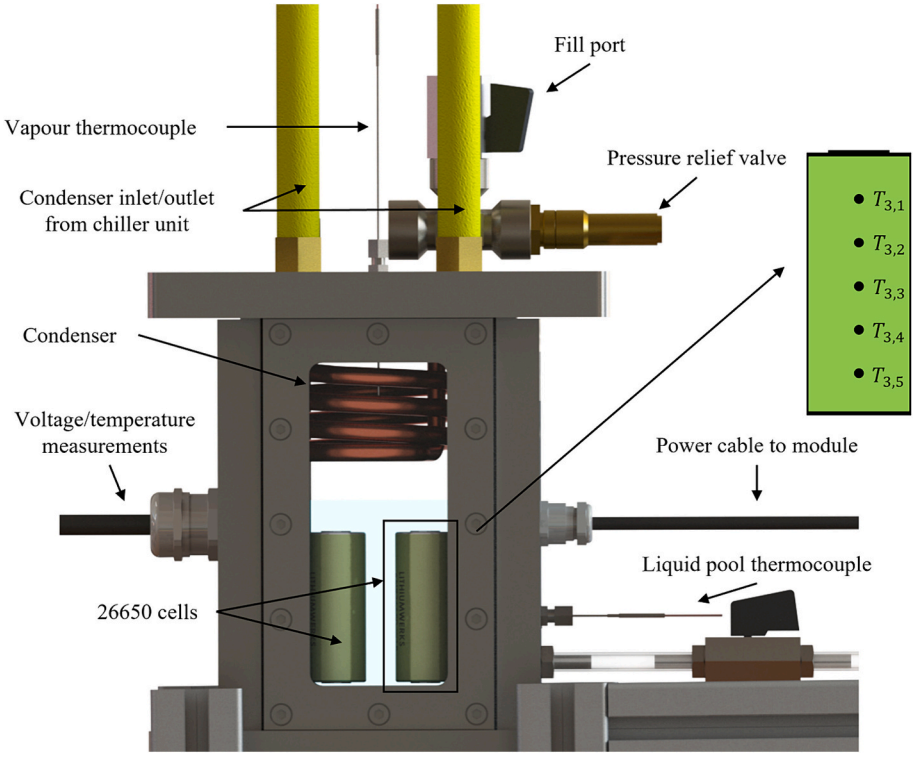

Fig. 2. 3D CAD render of the test chamber within the experimental set-up, including schematic of thermocouple locations on cells.

9214 DAQs.

The cell module is charged under constant current-constant voltage (CC-CV) conditions using a programable Elektro-Automatik EA-PSI 9080-60 T power supply. The maximum charge voltage during the CC stage is 3.6 V and the cell is considered fully charged (SOC = 1) when a current of 0.125 A is reached at the end of the CV stage. Module discharging is performed under CC conditions using a programmable Elektro-Automatik EA-EL 9080–45 T electronic load, ceasing when the cut-off voltage of 2 V is measured across the module. The current supplied to or drawn from the module is determined directly from the power supply and electronic load respectively. The module is rested for 1 h prior to a charging or discharging event at SOC's of 0 and 1 respectively, to allow for the open circuit voltage (OCV) to settle. Both the charging and discharging processes are controlled via bespoke NI LabVIEW programs, which also record all measurement parameters from the DAQs.

The performance of a cell or module can be described in terms of

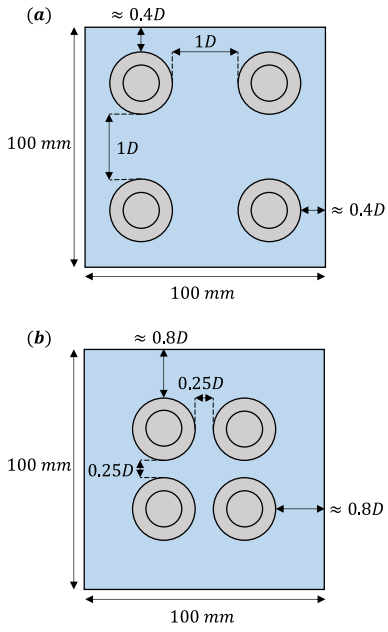

Fig. 3. Schematic of the numbered cells' arrangement within the module for spacings of (a) 1*D* and (b) 0.25*D*.

state of charge (SOC), which expresses the ratio of the available capacity to rated capacity as defined in Eq. (1), where t is the elapsed time during charging/discharging in seconds, I is the cell's operating current in A, and C_{cell} is the nominal capacity of the cell in Ah:

$$\mathrm{SOC(t)} = \mathrm{SOC(t_0)} + \int_0^t \frac{\mathrm{I}}{\mathrm{C_{cell}}}\,\mathrm{dt} \tag{1}$$

Fully depleted and fully charged cell states are represented by SOC values of 0 and 1 respectively. The discharge process is often described in terms of the depth of discharge or DOD, which is the converse of SOC:

$$\mathrm{DOD(t)} = 1 - \mathrm{SOC(t)} \tag{2}$$

2.2. Uncertainty reporting

Measurement uncertainty, also known as Type A uncertainty, as well as instrument uncertainty is used to determine the uncertainty of directly measured parameters such as the module's voltage. The precision error for the least-squares fit of the thermocouples' calibration is also considered. The uncertainty of the module's current measurement is taken to be the uncertainty associated with the power supply and electronic load. Table 3 reports the uncertainties determined.

3. Results and discussion

3.1. Module discharge

3.1.1. Temperature rise

The instantaneous surface averaged temperature increase $\Delta T_{i,avg}$ of a cell within the module with respect to its initial temperature $T_{i,avg}(t_0)$ can be described as in Eq. (3), where i is the cell number:

$$\Delta T_{i,avg} = T_{i,avg}(t) - T_{i,avg}(t_0) \tag{3}$$

The surface averaged temperature rise of Cell 1 during CC discharge is presented in Fig. 5 (a) and (b) for the cell spacings of 0.25*D* and 1*D* respectively, for single phase natural convection with initial ambient temperatures of 18.3 °C to 23.5 °C, and preheated fluid conditions of 33 °C ± 0.5 °C. $\Delta T_{1,avg}$ is observed to increase with both DOD and discharge rate for the spacing arrangements investigated. This arises as a greater internal overpotential η, which is the difference between the cell's OCV and terminal voltage and is realised as a loss in energy in the form of the irreversible heat, is produced by the higher current drawn. Additionally, the internal resistance of the cell rises throughout the discharge process, resulting in increasing η which reaches its maximum at the end of discharge.

The surface temperature rise, as well as the rate of that rise, is less pronounced under preheated immersion conditions as the phase change process provides more significant heat transfer. For the discharge rate of 1C, heat transfer through natural convection dominates as the cell surface does not exceed the fluid's saturation temperature. Conditions conducive to subcooled boiling are established for discharge rates of 2C and above, reaching saturated boiling conditions at the end of 3C and 4C discharge for the 1*D* spacing case as the fluid temperature rises above 34 °C. At these elevated temperatures, the cell's electrochemistry is more efficient as a result of increased electrolyte conductivity and electrode diffusivity, reducing the overpotential and as a consequence the heat generated, particularly at the end of discharge. This decrease in overpotential is reflected in the greater terminal voltages for preheated conditions, as seen in Fig. 5 (c). Furthermore, the phase change process can prevent excursions beyond this desirable operating range, which can lead to accelerated degradation from side reactions such as growth of the solid electrolyte interphase (SEI) layer.

The nucleation of vapour bubbles is observed from the surface of the electrodes only, consistent with the authors' previous work on single cell immersion cooling for the same cell-liquid combination [32]. Vapour bubble departure frequency is observed to increase with discharge rate. The localising of the boiling to the electrode surfaces is presumed to arise from the cell's greater axial thermal conductivity and the electrode's surface roughness, in addition to Joule heating from the electrical connections. As the electrochemical material within the cell is wound around a central mandrel, its thermal conductivity is

Table 1
Geometric, electrical, thermophysical properties of LithiumWerks ANR26650M1B $LiFePO_4$ cells.

Property	Value
Diameter	26 mm
Length	65 mm
Mass	76 g
Nominal capacity	2.5 Ah
Nominal voltage	3.3 V
Max. continuous current:	
Discharge	50 A (20C)
Charge	10 A (4C)
Density [36]	2047 kg/m^3
Specific heat [37]	1605 ± 80 J/kgK
Thermal conductivity [37]	
Axial	32 ± 1.6 W/mK
Radial	0.15 ± 0.01 W/mK
Heat generation rate (Natural convection conditions, 1C to 10C discharge) [38]	3 to 28 W

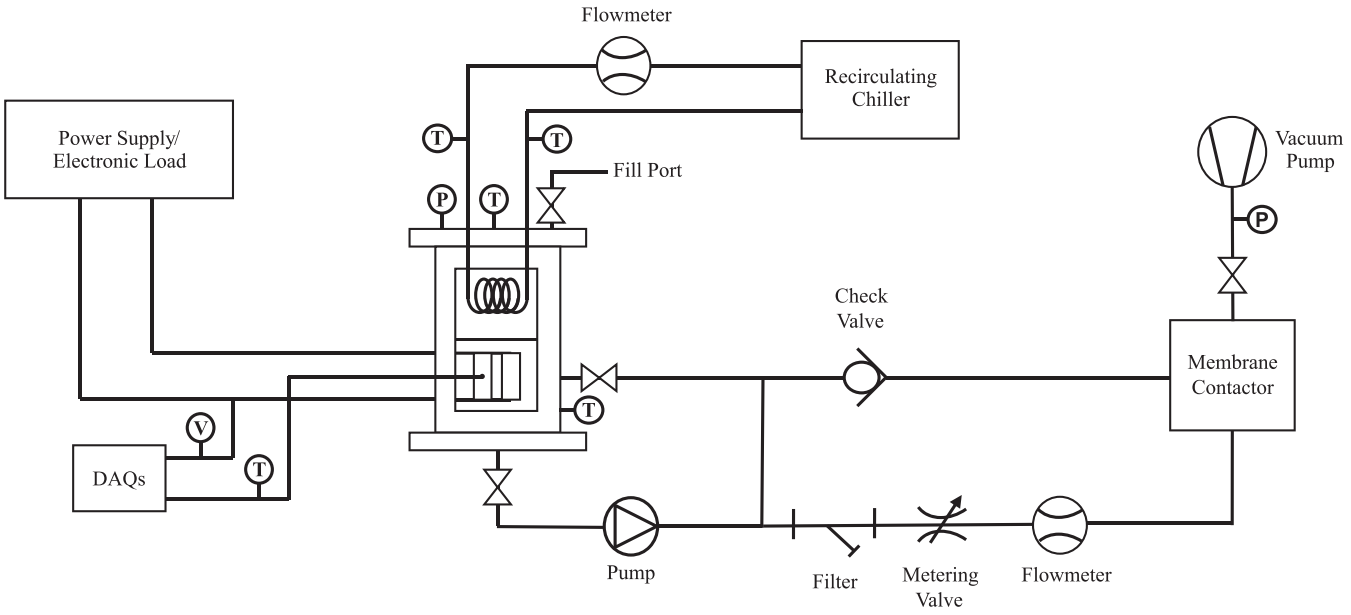

Fig. 4. Schematic of the experimental set-up.

Table 2
Thermophysical and electrical properties of 3M Novec 7000 at 25 °C.

Property	Value
Boiling point (1 atm)	34 °C
Liquid density	1400 kg/m^3
Kinematic viscosity	3.2×10^{-7} m^2/s
Specific heat	1300 J/kgK
Thermal conductivity	0.075 W/mK
Enthalpy of vaporisation	142 kJ/kg
Surface tension	0.0124 N/m
Dielectric strength	40 kV

Table 3
Measured and calculated parameter uncertainties.

Parameter	Uncertainty
Temperature	± 0.59 °C
Voltage	± 0.01 V
Charge Current	± 0.12 A
Discharge Current	± 0.09 A
Pressure	± 0.01 bar

significantly larger along its axis, as in Table 1, leading to greater heat flux on the electrode surface.

Furthermore, their increased surface roughness in comparison to the cylindrical surface yields a greater number of potential nucleation sites for vapour production, known to be a requirement for low viscosity dielectric fluids such as Novec 7000 [39]. As the electrodes serve as the contact location for the cell's electrical connections, some additional heat would be expected at these surfaces due to Joule heating. Immersion cooling may also be advantageous in maintaining the electrical connection components such as the busbars and cabling at lower temperatures, therefore reducing electrical losses.

Under preheated conditions, boiling first occurs on the lower electrode of the cell as greater heat is generated in the anode during the deintercalation process, dominated by the irreversible heat [40]. Vapour production is initiated at lower DOD values for increasing discharge rates, commencing immediately at the beginning of 4C discharge. The departure of smaller diameter vapour bubbles at greater frequency from the surface of the upper electrode is first observed for the 0.25*D* spacing arrangement at approximately 0.56 DOD during 2C discharge, as sufficient heat is generated by the cathode to induce boiling. As the discharge rate is increased, the greater overpotentials lead to more irreversible heat at the cathode, and earlier vapour incipience at 0.19 DOD and 0.14 DOD for 3C and 4C discharge respectively. The saturation conditions remain constant throughout all discharge cases for both spacings when two-phase conditions are established, with the pressure in the chamber maintained at 1 bar ± 0.02 bar. While not measured in this work, the electrode temperatures were previously determined for the case of a single cell under the same preheated immersion conditions. The lower electrode temperature remained approximately 0.8 °C above the average surface temperature throughout the discharge process at a rate of 4C.

Greater surface averaged cell temperature increases are determined under single phase natural convection conditions for 1*D* spacing in comparison to 0.25*D* spacing, except at 1C discharge. Maximum temperature rises of 7 °C and 7.8 °C occur at the end of 4C discharge for spacings of 0.25*D* and 1*D* respectively, corresponding to temperatures of 25.5 °C and 27.2 °C. The low viscosity of the dielectric fluid enhances instability within the flow, with turbulent natural convection conditions developing at the highest discharge rate as the surface and bulk fluid temperature difference increases. The greater mixing offered by this regime is experienced more intensely when the cell spacing is at its closest, leading to lower temperature rises. However, this behaviour requires further investigation for larger cell modules in which the portion of the cells' surface influenced by neighbouring cells will not be uniform.

Under the preheated conditions, the establishment of boiling on the electrodes, the locations of greatest heat generation, leads to more effective heat removal and lower cell temperatures. Additionally, the rising vapour from the lower electrodes disturbs the thermal boundary layers of the cells, further improving the heat transfer rate. For preheated conditions, lower surface averaged cell temperature rises are determined for the more closely arranged cells in the 0.25*D* spacing case, with Cell 1 temperature rises of 1.9 °C and 2.4 °C, corresponding to maximum temperatures of 34.7 °C and 36 °C, for the 0.25*D* and 1*D* spacings respectively at the same discharge rate of 4C. It is postulated that greater heat transfer occurs for the more closely spaced case as the vapour generated from the surface of the lower electrodes of neighbouring cells interacts while rising towards the liquid pool's surface. This interaction has the effect of creating greater mixing in the

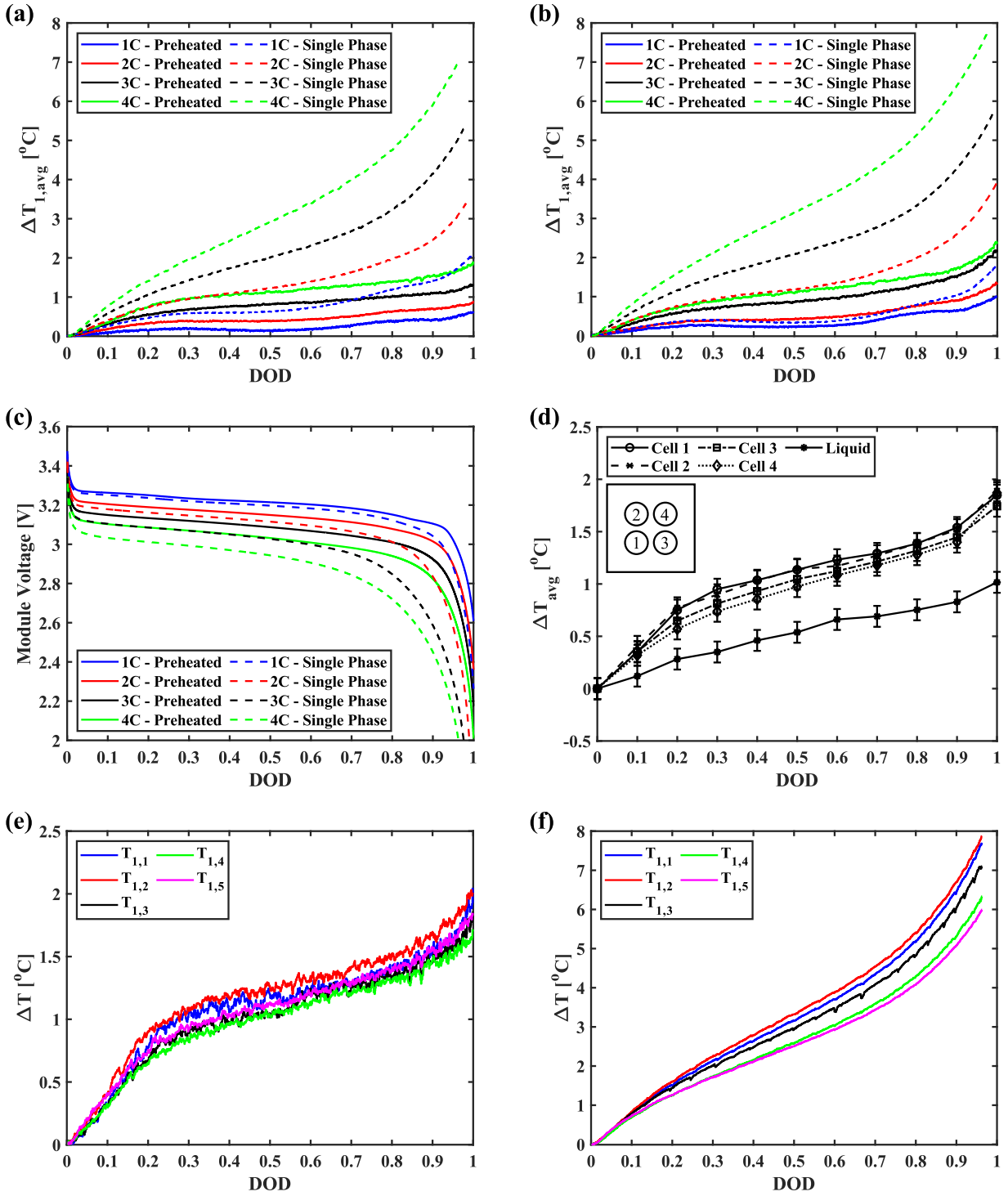

Fig. 5. Average surface temperature rise of Cell 1 under single phase natural convection and preheated conditions for 1C to 4C discharge at cell spacings of (a) 0.25*D* and (b) 1*D*. Voltage profiles of the module under single phase natural convection and preheated conditions for (c) 1C to 4C discharge and a cell spacing of 0.25*D*, (d) average surface temperature rise for all cells within module under preheated immersion conditions for 0.25*D* spacing at 4C discharge, including bulk fluid temperature rise and relative uncertainty of temperature measurements. Temperature rise of all thermocouples on Cell 1 for 4C discharge and a cell spacing of 0.25*D* for (e) preheated and (f) single phase natural convection conditions.

interstitial region between the cells and disturbing their thermal boundary layers more significantly. However, further work is required to better determine this behaviour.

All cells within the module are maintained below the recommended operating limit of 40 °C for the discharge rates investigated. Fig. 5 (d) presents the average surface temperature rise for all cells in the 0.25*D* spacing arrangement at a discharge rate of 4C under preheated immersion conditions. Cell 2 experienced the greatest temperature increase of 1.9 °C, corresponding to a surface temperature of 34.7 °C.

3.1.2. *Voltage profiles*

The module voltage profiles during discharge for both single phase natural convection and preheated conditions are presented in Fig. 5 (c) for a spacing of 0.25*D* only, as cell spacing is observed to have little

influence on the voltage behaviour. The sharp decrease in the profiles at the extremes of the discharge process, more evident as a DOD of 1 is approached, arise due to increased cell internal resistance, resulting in higher heat generation rates which are reflected in the corresponding temperature rises of Fig. 5 (a). Greater overpotentials are produced within the cells for increasing discharge rates, reflected in the module's reduced terminal voltage.

The duration of the discharge process, and therefore the module's usable capacity, is greater for all discharge rates under preheated conditions as a higher voltage is maintained in comparison to single phase natural convection conditions due to the reduced overpotential. The rapid decay of the voltage profile at the end of discharge is also approached notably later, as the temperature-sensitive electrochemical reactions are more efficient at higher temperatures. By increasing the duration and terminal voltage of the discharge process a greater electrical power can be delivered by the module, desirable for EV applications.

3.1.3. Thermal homogeneity

Temperature differences both across individual cells and between cells within a module develop during the charging and discharging processes. An important criterion of any proposed BTMS is the minimisation of these temperature differences to mitigate against accelerated degradation that results from imbalances both internal to the cell as well as cell-to-cell. The maximum temperature difference across a cell $\delta T_{i,max}$ can be expressed as the maximum instantaneous difference between the cell's temperature measurements, as in Eq. (4):

$$\delta T_{i,max} = T_{i,max}(t) - T_{i,min}(t) \tag{4}$$

The maximum temperature difference across the module δT_{module} is determined as the instantaneous maximum difference between the temperature measurements of all cells. The subscripts i and j refers to different cell numbers:

$$\delta T_{module} = T_{i,max}(t) - T_{j,min}(t) \tag{5}$$

Fig. 6 presents the maximum temperature difference across Cell 1, $\delta T_{1,max}$, and the maximum module temperature difference δT_{module} for both spacing arrangements investigated. Greater temperature differences across the individual cell are observed under single phase natural convection conditions, with similar temperatures differences determined for both spacing arrangements. For the 1D spacing arrangement shown in Fig. 6 (b), a maximum temperature difference of 2 °C is determined across Cell 1 at the end of 4C discharge, at the limit to minimise cell degradation.

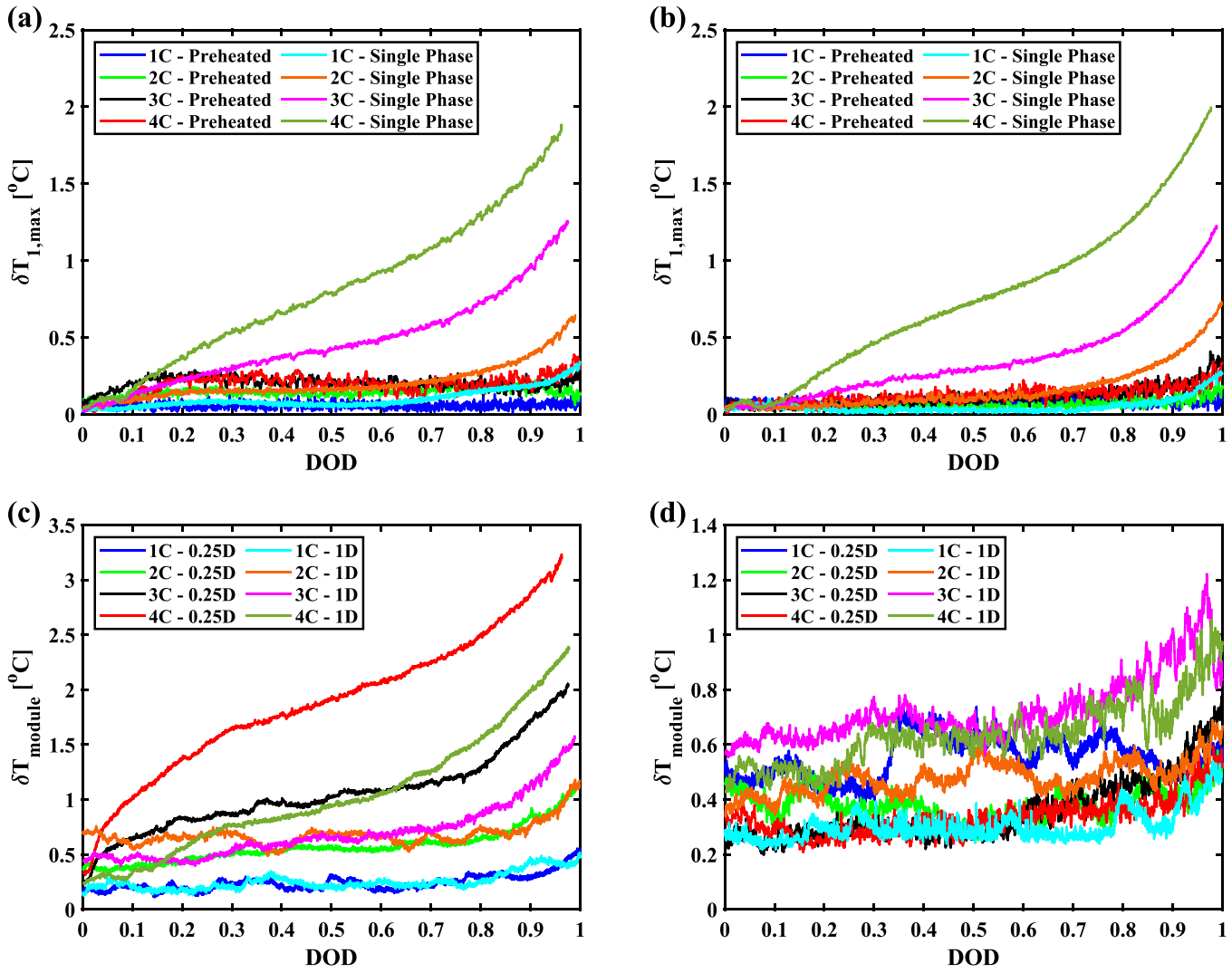

Fig. 6. Maximum temperature difference across Cell 1 for (a) 0.25D and (b) 1D spacing, and maximum module temperature difference under (c) single phase natural convection and (d) preheated conditions, for 1C to 4C discharge.

Fig. 5 (f) illustrates all temperature measurements across Cell 1 for the same conditions at 0.25*D* spacing, corresponding to $\delta T_{1,max}$ of Fig. 6 (a). A notable axial gradient is established between the upper and lower electrodes at a DOD of approximately 0.2, which continues to grow throughout the discharge process in response to the high polarization of the cell and the natural convection thermal boundary layer. In contrast, preheated immersion cooling exhibits excellent cell thermal homogeneity, maintaining $\delta T_{1,max}$ below 0.5 °C for all discharge rates and spacing arrangements investigated. As illustrated in Fig. 5 (e) for Cell 1 during 4C discharge at 0.25*D* spacing, the axial gradient is significantly reduced by the two-phase process, with the increased mixing and boundary layer disturbance induced by the vapour providing greater rates of heat transfer.

While the surface temperature gradient is used to illustrate the thermal homogeneity of the cell under the mechanisms of heat transfer investigated, it should be noted that a temperature difference will exist between the surface and inner core arising from the poor radial conductivity. The inner core temperature was not investigated in this study due to issues surrounding the resealing of the cells against the dielectric fluid such that the electrochemistry is unaffected. This may be examined in future studies in combination with numerical modelling of the cell.

Single phase natural convection conditions provide adequate cooling to maintain $\delta T_{module,max}$ below 5 °C for all discharge rates investigated, as in Fig. 6 (c), with a maximum module temperature difference of 3.2 °C observed at 4C discharge for the 0.25*D* spacing. Greater module temperature differences are determined for 3C and 4C discharge at this 0.25*D* spacing compared to 1*D*, whereas differences at the lower discharge rates of 1C and 2C are within measurement uncertainty (see Table 3).

A marked improvement is observed for preheated conditions as illustrated in Fig. 6 (d), with a maximum value of 1.2 °C for $\delta T_{module,max}$ at the end of 3C discharge for the 1*D* spacing case. This arises as the absorption of the heat generated through the latent heat of the dielectric fluid during the phase change process provides greater thermal homogenisation, both between cells and along their axes. In contrast to the single phase natural convection conditions, lower module temperature differences are determined for the more closely arranged cells under preheated conditions. However, the thermal inhomogeneity determined for 1*D* spacing is not substantially larger than for the more compact arrangement of 0.25*D*, approximately 0.5 °C higher at the discharge rate of 4C. Furthermore, this is of the order of the measurement uncertainty of the thermocouples. When considered with the average surface temperature rise of Fig. 5 (a) and (b), it appears that the closer spacing of 0.25*D* is preferable for more effective thermal management when employing two-phase immersion cooling. However, further work is required to investigate this behaviour in greater detail. No effect of the condensate reflux on the cells' temperature measurements, and therefore the thermal homogeneity, is observed under both module charging and discharging, as the height of the liquid pool is 15 mm above the cells' upper electrode.

3.2. Module charge

3.2.1. Temperature rise

Fig. 7 (a) and (b) presents $\Delta T_{1,avg}$ for CC-CV charging under single phase natural convection conditions at ambient temperatures between 22.7 °C and 24.2 °C, and preheated conditions of 33 °C ± 0.5 °C. Charging rates of 1C to 4C are investigated for both cell spacing arrangements. The cell average surface temperature is observed to increase with SOC throughout the CC stage of the charging process, as the module's terminal voltage, and as a consequence the overpotential and irreversible heat, rises towards the charging limit. As the CV stage progresses, an ever-reducing current is required to maintain the charge voltage limit as the cells' internal resistance continuously increases, illustrated in the corresponding voltage and current profiles of Fig. 7 (c) and (d). The reduction in charge current at the beginning of the CV charging stage, and therefore the irreversible heat generation, is not at first sufficient to cause an immediate decrease in the cell surface temperature, as the radial thermal conductivity is low. As an SOC of 1 is approached, the average cell temperature rapidly decreases in response to the reduced irreversible heat generation and the high heat transfer to the immersion fluid. The reversible heat generation of lithium-ion cells, dictated by the entropic heat coefficient $\frac{dU}{dT}$, is known to be of significance at low SOC. As this coefficient is negative at the beginning of the charging process, the reversible heat generation, and therefore the overall heat generation, is endothermic and results in an initial decrease in the average surface temperature as exhibited in Fig. 7 (a) and (b). The reversible heat generation is less influential for increasing C rates, leading to lower reductions in temperature upon charging initiation.

In a similar manner to the discharge process, lower maximum cell temperature increases occur under preheated conditions as a result of the high heat transfer rates during phase change, particularly at the electrode. The cell surface exceeds the saturation temperature at a charge rate of 2C and above in the 1*D* spacing arrangement under preheated conditions, and during 3C and 4C charging in the 0.25*D* spacing case, establishing subcooled boiling. Vapour bubble nucleation increases in intensity with charging rate, as greater heat is generated by the module's cells in response to the higher applied current. Vapour bubble production is first observed from the lower electrode at a rate of 2C, nucleating at lower SOC values for increasing C rates and appearing immediately upon initiation of charging at 4C due to high cell polarization. For the 1*D* spacing case, boiling is first observed from the upper electrodes at approximately 0.27 SOC at the same charging rate, becoming extremely vigorous at an SOC of 0.62 as the average cell temperature exceeds the saturation temperature. During the CV stage, the irreversible and total heat generation of the cells markedly decrease as the current decays towards its cut-off criteria at 0.125 A. This significantly reduces the heat flux at the upper electrode to such an extent that boiling is no longer sustained on that surface. The chamber pressure is maintained at 1 bar ±0.02 bar for both spacings when two-phase conditions are established, which are similar saturation conditions to those of the discharge cases.

Temperature increases during the CC stage are comparable to those experienced by the cell during the equivalent period of the discharging process for both immersion conditions. Similar quantities of heat are generated due to the dominance of the irreversible heat, which is dependent upon the current supplied to or drawn from the cell and the overpotential, which is of equivalent intensity for both processes. However, during the CV stage of charging, the cell's temperature plateaus before dropping sharply, as the irreversible heat continuously decreases in response to the reduced applied current. The reversible heat will also fall during this stage, contributing to the diminished total heat generation. In contrast, the temperature continues to rise throughout discharge as evident in Fig. 5., as the operating current remains constant and the terminal voltage decays rapidly, inducing significant overpotentials.

The influence of spacing on the cell's maximum temperature rise is found to be minimal for single phase natural convection cooling. Under preheated conditions the spacing of 1*D* produces greater temperature rises at each C rate, with a maximum of approximately 1.8 °C, corresponding to a temperature of 34.8 °C, during 4C charging. In comparison, a maximum temperature rise of 1.3 °C occurs for the 0.25*D* spacing at the same charging rate, equivalent to 35 °C. As in the preheated discharge case, the greater proximity of the cells is presumed to allow for greater vapour interaction and mixing, enhancing heat transfer from the cell's surface. However, these cell temperature increases under charging

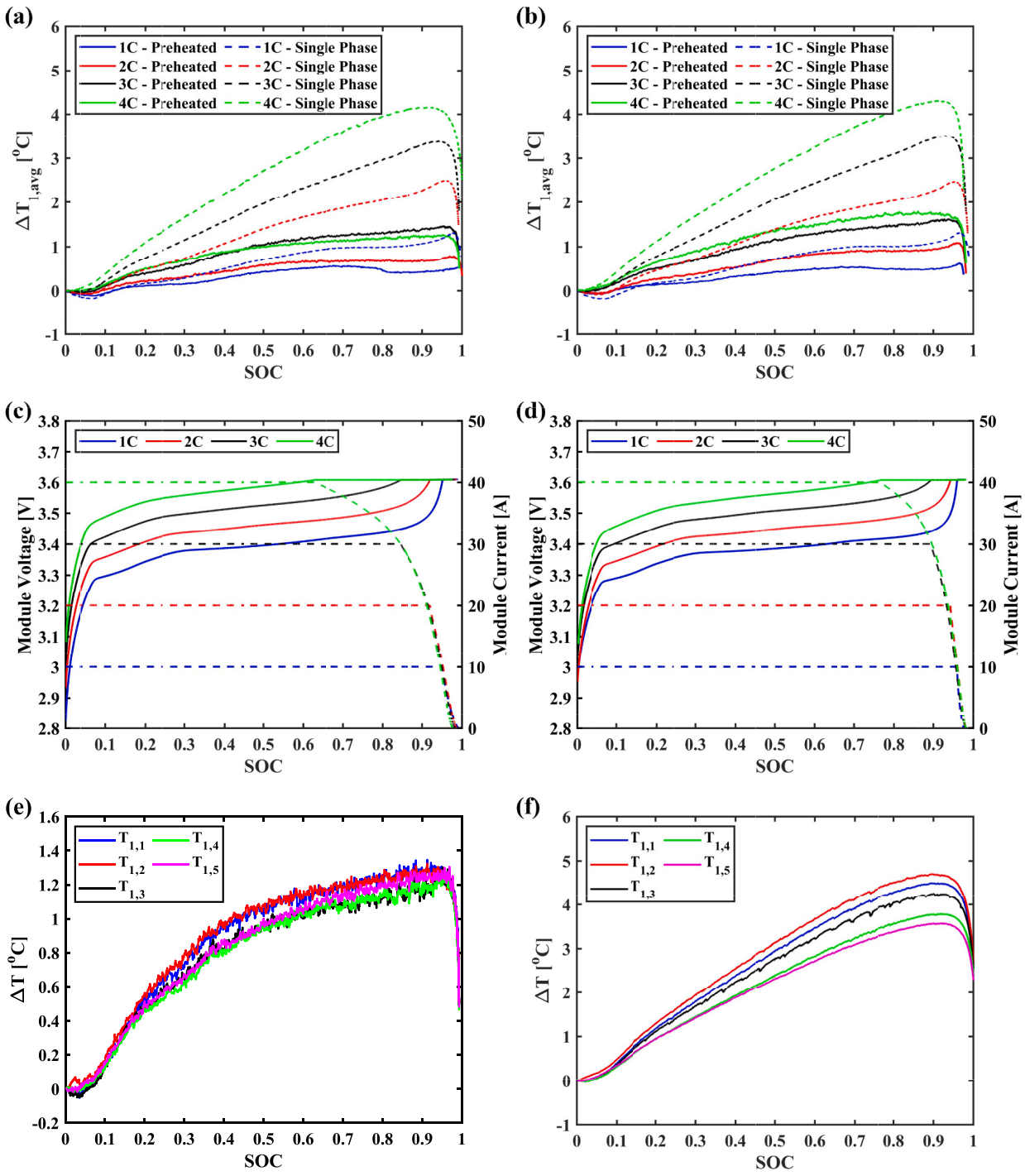

Fig. 7. Average surface temperature rise of Cell 1 under single phase natural convection and preheated conditions at charge rates of 1C to 4C for cell spacings of (a) 0.25*D* and (b) 1*D*. Voltage (solid lines) and current (dashed lines) profiles of the module during 1C to 4C charging for 1*D* spacing under (c) single phase natural convection and (d) preheated immersion cooling conditions, and temperature rise of all thermocouples on Cell 1 for 4C charge and a cell spacing of 0.25*D* for (e) preheated and (f) single phase natural convection conditions.

are lower in comparison to $\Delta T_{1,avg}$ for the equivalent discharge case due to the reduced heat generation, as previously discussed.

The average surface temperature rise during 4C charging under preheated conditions is presented in Fig. 8 for the spacing of 0.25*D*. All cells remain below the operating limit, with the maximum temperature increase of 1.5 °C experienced by Cell 4. The required operating temperature limits are maintained under both immersion conditions and for the two cell spacing arrangements throughout the charge rates investigated, further illustrating the suitability of immersion cooling for battery thermal management.

3.2.2. *Voltage and current profiles*

Module voltage and current profiles under both single phase natural convection and preheated conditions are presented in Fig. 7 (c) and (d) for the cell spacing of 1*D*. The duration of the CC stage reduces for increasing C rate, as the upper voltage limit is reached more quickly in the charging process due to the greater overpotentials developed within the cells in response to the higher charge current.

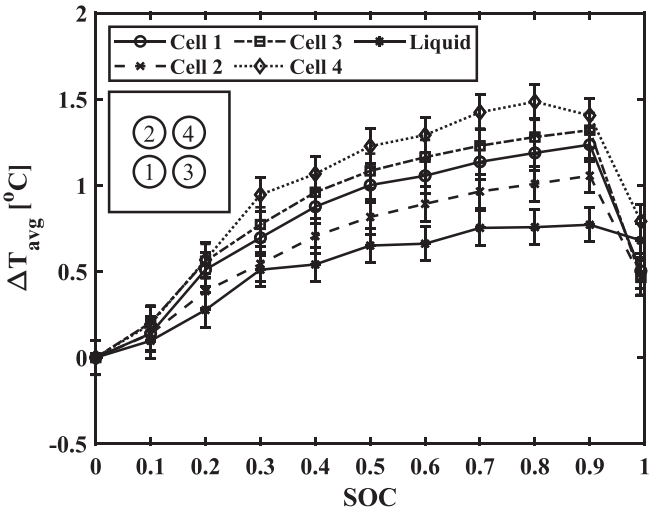

Fig. 8. Average surface temperature rise of all cells within the module for 0.25*D* spacing at a charge rate of 4C under preheated conditions, including bulk fluid temperature rise and relative uncertainty of temperature measurements.

Lower charging voltages are required for equivalent SOC values under preheated conditions as the electrochemical reactions are more efficient at these elevated temperatures, decreasing the cells' internal resistance and overpotential. The CV stages are of shorter duration as in Fig. 7 (d), accompanied by a reduction in charging times. This is particularly evident at the fast charging rate of 4C as the CC stage is significantly extended under preheated conditions, terminating at an SOC of approximately 0.76 in comparison to an SOC of approximately 0.63 under single phase natural convection conditions. With regard to total charging time, the module is considered fully charged after approximately 1201 s and 1329 s for preheated and single phase natural convection conditions respectively.

The advantageous performance of immersion cooling is particularly evident for the charging process, as cells can be maintained at temperatures which allow for more efficient and shorter duration charging, without exceeding the operating temperature limits.

3.2.3. *Thermal homogeneity*

The maximum temperature differences across both Cell 1 and the module during CC-CV charging are presented in Fig. 9 for the spacing arrangements of 0.25*D* and 1*D*. In a similar manner to the discharge cases, greater temperature differences are observed across the individual cell under single phase natural convection conditions as the rates of heat

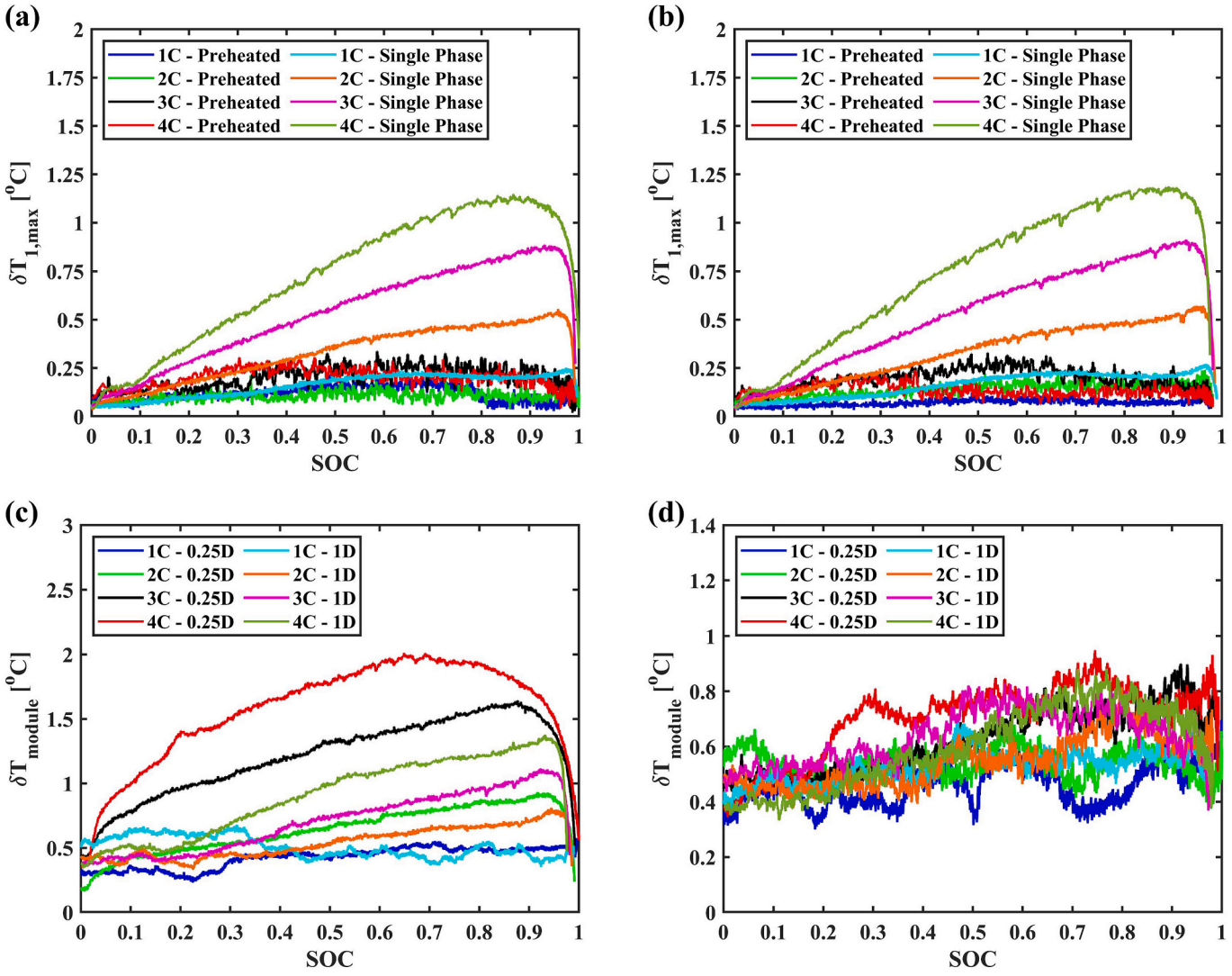

Fig. 9. Maximum temperature difference across Cell 1 for (a) 0.25*D* and (b) 1*D* spacing and maximum temperature difference across the module under (c) single phase natural convection and (d) preheated conditions for 1C to 4C charge.

transfer are much reduced. Comparable values for $\delta T_{1,max}$ are determined for both spacing arrangements at all charge rates, limited to 1.2 °C during the most onerous rate of 4C as in Fig. 9 (a) and (b). This axial thermal gradient is illustrated in Fig. 7 (f), which remains relatively constant at the initiation of the CV stage, despite the reduction in the heat generation rate, as the poor radial thermal conductivity prevents the temperature from changing rapidly. As the CV stage continues, the less intense electrochemical reactions within the cell lowers the axial thermal gradient to 0.2 °C by the end of the charging process.

Improved performance occurs under preheated conditions, with $\delta T_{1,max}$ of 0.3 °C and 0.2 °C for 0.25*D* and 1*D* spacing respectively, as the vapour can significantly agitate the fluid in the vicinity of the cell surface as it rises from the lower electrode. No significant influence of cell spacing on individual cell temperature differences is observed, with Fig. 7 (e) illustrating the low axial gradient which develops between the electrodes at a charge rate of 4C under the enhanced heat transfer conditions.

Immersion cooling provides excellent thermal uniformity for both cooling conditions, with δT_{module} reaching a maximum for all charge cases of approximately 2 °C under natural convection during 4C charging. The beneficial performance of the dielectric fluid's phase change is again illustrated under preheated conditions, limiting δT_{module} to less than 1 °C for all charge rates investigated. The cell spacing exhibits little influence on δT_{module} under preheated conditions, with variations between the two arrangements not exceeding 0.1 °C. Larger module temperature differences are found for the 0.25*D* spacing during 3C and 4C charging under single phase natural convection conditions.

4. Conclusion

The thermal management of a 26650 $LiFePO_4$ cylindrical four cell module through direct contact liquid immersion cooling was experimentally investigated in this study, for complete immersion in the dielectric fluid Novec 7000. The thermal and electrical performance of the module was assessed for charging and discharging rates of up to 4C, under both single phase natural convection conditions and two-phase conditions when the fluid was preheated to 33 °C ± 0.5 °C. The effect of cell spacing within the module was also investigated for inter-cell spacings of 0.25*D* and 1*D*, where *D* is the cell's diameter. The cells of the module were maintained below the required operating temperature limit for lithium-ion cells of 40 °C at all charge and discharge rates investigated under both cooling conditions. Improved thermal and electrical performance was observed for preheated conditions, as the phase change process significantly increased the rate of heat transfer, leading to lower cell average temperature rises and superior thermal homogenisation in comparison to single phase natural convection conditions. Maximum average surface temperature rises of 1.9 °C and 1.3 °C, equivalent to maximum temperatures of 34.7 °C and 35 °C, were determined for an individual cell within the model for discharging and charging at 4C respectively under preheated conditions, with corresponding maximum temperature differences across the module of 0.6 °C and 1 °C. During the phase change, vapour bubble nucleation was concentrated on the upper and lower electrodes of the cells, departing the surface more frequently for increasing charge and discharge rates and enhancing the heat transfer through increased fluid agitation. Slightly improved performance was observed for the more closely spaced cell arrangement of 0.25*D*, as increased interaction between the vapour produced by neighbouring cells during the phase change process led to greater fluid agitation and lower surface temperatures. Future work will subject the module to drive cycling conditions which more closely replicate the demands placed on a BTMS, expanding the module design to include a greater number of cells, as well as the development of a coupled electrochemical-thermal numerical model.

CRediT authorship contribution statement

N.P. Williams: Writing – review & editing, Writing – original draft, Visualization, Methodology, Investigation, Conceptualization. **D. Trimble:** Supervision, Project administration, Methodology, Funding acquisition, Conceptualization. **S.M. O'Shaughnessy:** Writing – review & editing, Writing – original draft, Supervision, Project administration, Methodology, Funding acquisition, Conceptualization.

Declaration of competing interest

The authors declare the following financial interests/personal relationships which may be considered as potential competing interests: Seamus O'Shaughnessy reports financial support was provided by Science Foundation Ireland. If there are other authors, they declare that they have no known competing financial interests or personal relationships that could have appeared to influence the work reported in this paper.

Data availability

Data will be made available on request.

Acknowledgement

The authors gratefully acknowledge the financial support from Trinity College Dublin's Provost's PhD Project Award and Research Boost Programme, and Science Foundation Ireland (SFI) 2050 Challenge Award 22/NCF/TF/10952. Our experimental work is supported by computational simulations carried out on the Irish Centre for High End Computing (ICHEC) under project ID tceng054c.

Appendix A. Supplementary data

Supplementary data to this article can be found online at https://doi.org/10.1016/j.est.2024.111289.

References

[1] A.A. Pesaran, Battery thermal models for hybrid vehicle simulations, J. Power Sources 110 (2) (2002) 377–382, https://doi.org/10.1016/S0378-7753(02)00200-8.
[2] R. Carter, et al., Directionality of thermal gradients in lithium-ion batteries dictates diverging degradation modes, Cell Rep. Phys. Sci. 2 (3) (2021) 100351, https://doi.org/10.1016/j.xcrp.2021.100351.
[3] S. Paul, C. Diegelmann, H. Kabza, W. Tillmetz, Analysis of ageing inhomogeneities in lithium-ion battery systems, J. Power Sources 239 (2013) 642–650, https://doi.org/10.1016/j.jpowsour.2013.01.068.
[4] F.M.N.U. Khan, M.G. Rasul, A.S.M. Sayem, N.K. Mandal, Design and optimization of lithium-ion battery as an efficient energy storage device for electric vehicles: a comprehensive review, J. Energy Storage 71 (2023) 108033, https://doi.org/10.1016/j.est.2023.108033.
[5] J. Deng, C. Bae, A. Denlinger, T. Miller, Electric vehicles batteries: requirements and challenges, Joule 4 (3) (2020) 511–515, https://doi.org/10.1016/j.joule.2020.01.013.
[6] Y. Chen, J.W. Evans, Heat transfer phenomena in lithium/polymer-electrolyte batteries for electric vehicle application, J. Electrochem. Soc. 140 (7) (1993) 1833–1838, https://doi.org/10.1149/1.2220724.
[7] Y. Liu, J. Zhang, Design a J-type air-based battery thermal management system through surrogate-based optimization, Appl. Energy 252 (2019) 113426, https://doi.org/10.1016/j.apenergy.2019.113426.
[8] M. Malik, I. Dincer, M.A. Rosen, M. Mathew, M. Fowler, Thermal and electrical performance evaluations of series connected Li-ion batteries in a pack with liquid cooling, Appl. Therm. Eng. 129 (2018) 472–481, https://doi.org/10.1016/j.applthermaleng.2017.10.029.
[9] M.S. Patil, J.H. Seo, S. Panchal, S.W. Jee, M.Y. Lee, Investigation on thermal performance of water-cooled Li-ion pouch cell and pack at high discharge rate with U-turn type microchannel cold plate, Int. J. Heat Mass Transf. 155 (2020) 119728, https://doi.org/10.1016/j.ijheatmasstransfer.2020.119728.
[10] P. Nelson, D. Dees, K. Amine, G. Henriksen, Modeling thermal management of lithium-ion PNGV batteries, J. Power Sources 110 (2) (2002) 349–356, https://doi.org/10.1016/S0378-7753(02)00197-0.

[11] A. Babapoor, M. Azizi, G. Karimi, Thermal management of a Li-ion battery using carbon fiber-PCM composites, Appl. Therm. Eng. 82 (2015) 281–290, https://doi.org/10.1016/j.applthermaleng.2015.02.068.
[12] Z. Rao, Y. Huo, X. Liu, Experimental study of an OHP-cooled thermal management system for electric vehicle power battery, Exp. Thermal Fluid Sci. 57 (2014) 20–26, https://doi.org/10.1016/j.expthermflusci.2014.03.017.
[13] D.W. Sundin, S. Sponholtz, Thermal management of Li-ion batteries with single-phase liquid immersion cooling, IEEE Open J. Vehic. Technol. 1 (2020) 82–92, https://doi.org/10.1109/OJVT.2020.2972541.
[14] S. Hemavathi, S. Srinivas, A.S. Prakash, Performance evaluation of a hydrostatic flow immersion cooling system for high-current discharge Li-ion batteries, J. Energy Storage 72 (2023) 108560, https://doi.org/10.1016/j.est.2023.108560.
[15] G. Satyanarayana, D. Ruben Sudhakar, V. Muthya Goud, J. Ramesh, G. A. Pathanjali, Experimental investigation and comparative analysis of immersion cooling of lithium-ion batteries using mineral and therminol oil, Appl. Therm. Eng. 225 (2023) 120187, https://doi.org/10.1016/j.applthermaleng.2023.120187.
[16] J. Liu, Q. Ma, X. Li, Numerical study on heat dissipation performance of a lithium-ion battery module based on immersion cooling, J. Energy Storage 66 (2023) 107511, https://doi.org/10.1016/j.est.2023.107511.
[17] H. Wang, T. Tao, J. Xu, H. Shi, X. Mei, P. Gou, Thermal performance of a liquid-immersed battery thermal management system for lithium-ion pouch batteries, J. Energy Storage 46 (2022) 103835, https://doi.org/10.1016/j.est.2021.103835.
[18] M.S. Patil, J.H. Seo, M.Y. Lee, A novel dielectric fluid immersion cooling technology for Li-ion battery thermal management, Energy Convers. Manag. 229 (2021) 113715, https://doi.org/10.1016/j.enconman.2020.113715.
[19] Y. Zha, S. He, X. Meng, H. Zuo, X. Zhao, Heat dissipation performance research between drop contact and immersion contact of lithium-ion battery cooling, Energy 279 (2023) 128126, https://doi.org/10.1016/j.energy.2023.128126.
[20] Y. Liu, G. Aldan, X. Huang, M. Hao, Single-phase static immersion cooling for cylindrical lithium-ion battery module, Appl. Therm. Eng. 233 (2023) 121184, https://doi.org/10.1016/j.applthermaleng.2023.121184.
[21] D. Koster, A. Marongiu, D. Chahardahcherik, C.F. Braun, D. Schulte, E. Figgemeier, Degradation analysis of 18650 cylindrical cell battery pack with immersion liquid cooling system. Part 1: aging assessment at pack level, J. Energy Storage 62 (2023) 106839, https://doi.org/10.1016/j.est.2023.106839.
[22] H. Choi, H. Lee, J. Kim, H. Lee, Hybrid single-phase immersion cooling structure for battery thermal management under fast-charging conditions, Energy Convers. Manag. 287 (2023) 117053, https://doi.org/10.1016/j.enconman.2023.117053.
[23] E. Solai, M. Guadagnini, H. Beaugendre, R. Daccord, P. Congedo, Validation of a data-driven fast numerical model to simulate the immersion cooling of a lithium-ion battery pack, Energy 249 (2022) 123633, https://doi.org/10.1016/j.energy.2022.123633.
[24] J. W. Han, K. S. Garud, S. G. Hwang, and M. Y. Lee, "Experimental study on dielectric fluid immersion cooling for thermal management of lithium-ion battery," Symmetry, 14, 10, p. 2126 https://doi.org/10.3390/sym14102126.
[25] L. Giammichele, V. D'Alessandro, M. Falone, R. Ricci, Experimental study of a direct immersion liquid cooling of a Li-ion battery for electric vehicles applications, Int. J. Heat Technol. 40 (1) (2022) 1–8, https://doi.org/10.18280/ijht.400101.
[26] R.W. van Gils, D. Danilov, P.H.L. Notten, M.F.M. Speetjens, H. Nijmeijer, Battery thermal management by boiling heat-transfer, Energy Convers. Manag. 79 (2014) 9–17, https://doi.org/10.1016/j.enconman.2013.12.006.
[27] Y. Li, et al., Experimental studies of liquid immersion cooling for 18650 lithium-ion battery under different discharging conditions, Case Stud. Therm. Eng. 34 (2022) 102034, https://doi.org/10.1016/j.csite.2022.102034.
[28] L. Giammichele, V. D'Alessandro, M. Falone, R. Ricci, Preliminary analysis of a novel battery thermal management system based on a low boiling dielectric fluid, IOP Conf. Ser. Earth Environ. Sci. 1106 (1) (2022) 012017, https://doi.org/10.1088/1755-1315/1106/1/012017.
[29] H. Hirano, T. Tajima, T. Hasegawa, T. Sekiguchi, M. Uchino, Boiling liquid battery cooling for electric vehicle, in: 2014 IEEE Conference and Expo Transportation Electrification Asia-Pacific (ITEC Asia-Pacific), 31 Aug.-3 Sept. 2014, 2014, pp. 1–4, https://doi.org/10.1109/ITEC-AP.2014.6940931.
[30] Y. Li, et al., Experimental study of liquid immersion cooling for different cylindrical lithium-ion batteries under rapid charging conditions, Therm. Sci. Eng. Prog. 37 (2023) 101569, https://doi.org/10.1016/j.tsep.2022.101569.
[31] Y. Li, et al., Experimental investigations of liquid immersion cooling for 18650 lithium-ion battery pack under fast charging conditions, Appl. Therm. Eng. 227 (2023) 120287, https://doi.org/10.1016/j.applthermaleng.2023.120287.
[32] N.P. Williams, D. Trimble, S.M. O'Shaughnessy, Liquid immersion thermal management of lithium-ion batteries for electric vehicles: an experimental study, J. Energy Storage 72 (2023) 108636, https://doi.org/10.1016/j.est.2023.108636.
[33] M. Al-Zareer, I. Dincer, M.A. Rosen, A novel approach for performance improvement of liquid to vapor based battery cooling systems, Energy Convers. Manag. 187 (2019) 191–204, https://doi.org/10.1016/j.enconman.2019.02.063.
[34] N. Wu, X. Ye, J. Yao, X. Zhang, X. Zhou, B. Yu, Efficient thermal management of the large-format pouch lithium-ion cell via the boiling-cooling system operated with intermittent flow, Int. J. Heat Mass Transf. 170 (2021) 121018, https://doi.org/10.1016/j.ijheatmasstransfer.2021.121018.
[35] Y.-F. Wang, et al., Experimental study on immersion phase change cooling of lithium-ion batteries based on R1233ZD(E)/ethanol mixed refrigerant, Appl. Therm. Eng. 220 (2023) 119649, https://doi.org/10.1016/j.applthermaleng.2022.119649.
[36] M. Xu, R. Wang, B. Reichman, X. Wang, Modeling the effect of two-stage fast charging protocol on thermal behavior and charging energy efficiency of lithium-ion batteries, J. Energy Storage 20 (2018) 298–309, https://doi.org/10.1016/j.est.2018.09.004.
[37] S.J. Drake, D.A. Wetz, J.K. Ostanek, S.P. Miller, J.M. Heinzel, A. Jain, Measurement of anisotropic thermophysical properties of cylindrical Li-ion cells, J. Power Sources 252 (2014) 298–304, https://doi.org/10.1016/j.jpowsour.2013.11.107.
[38] L. Giammichele, V. D'Alessandro, M. Falone, R. Ricci, Thermal behaviour assessment and electrical characterisation of a cylindrical Lithium-ion battery using infrared thermography, Appl. Therm. Eng. 205 (2022) 117974, https://doi.org/10.1016/j.applthermaleng.2021.117974.
[39] M.S. El-Genk, M. Pourghasemi, Experiments and correlations of saturation boiling of hfe-7000 dielectric liquid on rough inclined copper surfaces, Int. J. Heat Mass Transf. 164 (2021) 120540, https://doi.org/10.1016/j.ijheatmasstransfer.2020.120540.
[40] L. Wu, K. Liu, J. Liu, H. Pang, Evaluating the heat generation characteristics of cylindrical lithium-ion battery considering the discharge rates and N/P ratio, J. Energy Storage 64 (2023) 107182, https://doi.org/10.1016/j.est.2023.107182.